small methods
www.small-methods.com

A Self-Driven Ga_2O_3 Memristor Synapse for Humanoid Robot Learning

*Jianya Zhang, Jiamin Li, Rui Xu, Yudie Wang, Jiawen Wang, Tianxiang Wang, and Yukun Zhao**

In recent years, the rapid development of brain-inspired neuromorphic systems has created an imperative demand for artificial photonic synapses that operate with low power consumption. In this study, a self-driven memristor synapse based on gallium oxide (Ga_2O_3) nanowires is proposed and demonstrated successfully. This memristor synapse is capable of emulating a range of functionalities of biological synapses when exposed to 255 nm light stimulation. These functionalities encompass peak time-dependent plasticity, pulse facilitation, and memory learning capabilities. It exhibits an ultrahigh paired-pulse facilitation index of 158, indicating exceptional learning performance. The transition from short-term memory to long-term memory can be attributed to the remarkable relearning capabilities. Furthermore, the potential applications of the memristor synapse is showcased through the successful manipulation of a humanoid intelligent robot. Upon establishing artificial intelligence (AI) systems, the control commands originating from the synaptic device can drive the humanoid robot to perform various actions. Based on the memristor synapses, the autonomous feedback system of the humanoid robot facilitates a good collaboration between robotic actions and bio-inspired light perception. Therefore, this research opens up an effective way to advance the development of neuromorphic computing technologies, AI systems, and intelligent robots that demand ultra-low energy consumption.

1. Introduction

With the swift advancement of big data, the Internet of Things (IoT), and artificial intelligence (AI) in recent years, traditional computer systems have evolved to handle complex systems with greater sophistication, particularly those that require interaction with dynamic environments and navigating various uncertainties. The Neumann architecture, characterized by its distinct separation of memory and storage units, is increasingly unable to fulfill the requirements of future applications.[1–3] The human brain possesses extraordinary capabilities, attributed to its highly parallel, efficient, fault-tolerant, and reconfigurable neural network systems, which are capable of processing information with remarkable efficiency at ultra-low power consumption.[1,4] Inspired by the human brain, artificial optical memristor synapses have emerged and garnered significant interest for their capacity to process and memorize data concurrently.[5–7] By incorporating essential aspects of neuronal signal processing, memristors are capable of emulating the roles of conventional biological receptors, neurons, and synapses.[8] Upon exposure to light, optical synaptic devices exhibit several advantages, including high bandwidth, rapid signal transmission, strong robustness, and enhanced connectivity between discrete computing modules.[9–11] Furthermore, humanoid robots are extensively utilized across various sectors including healthcare, the service industry, education and entertainment, etc.[12] Therefore, the development of a light-stimulated memristor synapse, capable of emulating synaptic function, is crucial and indispensable for the advancement of humanoid robots.[13]

On the other hand, nanowires are regarded as an effective method to emulate artificial synaptic learning and cognition owing to their exceptional properties, including a large surface area ratio and substantial biological capacity.[14] With its ultrawide bandgap of 4.86 eV, gallium oxide (Ga_2O_3) holds significant promise in the realm of deep UV light, potentially enabling applications in secure communication.[15–17] Ga_2O_3 nanowires are anticipated to serve as potential candidates for artificial optical synapses, owing to their exceptional thermal and chemical stability.[17] Furthermore, the operation of self-driven devices has garnered considerable attention, which requires no external power source. This development could pave an effective way toward alleviating the energy crisis. Nevertheless, despite the

J. Zhang, J. Li, R. Xu, Y. Wang, J. Wang, T. Wang
Key Laboratory of Efficient Low-carbon Energy Conversion and Utilization of Jiangsu Provincial Higher Education Institutions
School of Physical Science and Technology
Suzhou University of Science and Technology
Suzhou 215009, China

J. Zhang, Y. Zhao
Division of Nano-Devices Research
Suzhou Institute of Nano-Tech and Nano-Bionics (SINANO)
Chinese Academy of Sciences (CAS)
Suzhou 215123, China
E-mail: ykzhao2017@sinano.ac.cn

Y. Zhao
School of Nano-Tech and Nano-Bionics
University of Science and Technology of China
Hefei 230026, China

The ORCID identification number(s) for the author(s) of this article can be found under https://doi.org/10.1002/smtd.202400989

DOI: 10.1002/smtd.202400989

existing research gap in self-driven Ga_2O_3-nanowire synaptic devices, the fabrication of a light-stimulated synaptic device for humanoid robot learning remains both challenging and appealing.

In our previous research, we fabricated GaN nanowires and developed photodetectors.[18,19] However, Ga_2O_3 nanowires have yet to be integrated into artificial synaptic devices, let alone utilized in the learning processes of humanoid robots. In this paper, we present evidence that a light-stimulated synaptic device utilizing Ga_2O_3 nanowires is capable of emulating various functions of biological synapses. These functions encompass paired-pulse facilitation (PPF), pulse-timing-dependent plasticity, as well as learning and memory functions. In addition, we set up an artificial neural system to govern the humanoid intelligent robot. This light-stimulated artificial memristor synapse is used to control the humanoid robot and has promising applications in fields such as AI systems and brain-mimicking chips, etc.

2. Experimental Section

2.1. Preparation of Ga_2O_3/GaN Nanowires and Synaptic Device

By using molecular beam epitaxy (MBE, Vecco G20), vertical GaN nanowire arrays (**Figure 1a**) were fabricated on n-type Si(111) substrates. In the MBE chamber, Si(111) was preheated to 900 °C for 15 min to remove the natural oxides. N atoms were supplied by the N plasma cell with a constant N flow rate (4.8 sccm) and plasma power (450 W). Ga atoms were supplied by the Ga effusion cell. In the growth process, a layer of ≈3 nm-thick AlN sacrificial layer was deposited on Si(111). Under a nominal Ga flux of $\approx 2.0 \times 10^{-8}$ Torr, the growth time of GaN nanowires was 110 min.

To prepare the Ga_2O_3 section, the GaN vertical nanowire arrays were exposed to oxygen gas at 800 °C for 10 min (Figure 1b). After fabricating the Ga_2O_3/GaN nanowires, the samples were cut into small pieces. The In/Au/Al alloys were melted on the Si back side to connect the conducting wire, which was coated by epoxy resin to avoid the leakage current and EC corrosion (Figure 1c).

2.2. Characterization and Measurements

A scanning electron microscope (SEM) was used to measure the morphology of Ga_2O_3/GaN nanowires. For aberration-corrected transmission electron microscopy (AC-STEM), samples were prepared by focused ion beam (FIB) for structural and elemental analysis. After that, an Agilent B1500A semiconductor parameter analyzer was used to characterize the synaptic functionality of the device. A 255 nm light-emitting diode (LED) was carried out as the lighting source for the response measurements. To characterize the chemical states and atomic binding states of the nanowires, X-ray photoelectron spectroscopy (XPS) was utilized.

2.3. Humanoid Intelligent Robot

The light-stimulated synaptic device was used as a simplified autonomous feedback system to emulate the multiple functions of biological synapses (Figure 1d). It was combined with the humanoid intelligent robot control system (Figure 1e) to demonstrate learning and memory ability. The whole humanoid intelligent robot system was divided into a front-end hardware system and a back-end remote intelligent control system, including a photoelectric conversion subsystem, data acquisition subsystem, signal processing subsystem, control decision subsystem, and action execution subsystem.

3. Results and Discussion

In the biological nervous system, the synapse is the site of functional contact between neurons and an important site of information transmission.[13] When the excitatory postsynaptic potential reaches the valve potential and triggers the postsynaptic neuron action potential to achieve information transmission, the nanowire-based synaptic device is designed to emulate the function of biological synapses. Under light stimulation, the production and transport of vectors in the artificial synaptic device are used to emulate the transport of neurotransmitters in biological synapses. The Ga_2O_3 nanowires perform the role of the synaptic cleft, and the surface of the device exposed to light acts as the presynaptic element (Figure 1d).[20] According to Figure 1f–h, the distribution of the O element demonstrates the effective oxidation of nanowires, leading to the Ga_2O_3/GaN hybrid nanowires. They agree well with the structural design.

The weight of synapses can be changed by regulating the activity of pre-synaptic and post-synaptic neurons, a property commonly referred to as synaptic plasticity.[21,22] It underlies much of the human brain's learning, forgetting, and reviewing ability.[23] In addition, paired-pulse facilitation (PPF) is a typical phenomenon of short-range plasticity, which is essential for decoding provisional information in the auditory and visual systems.[24] From **Figure 2a**, excitatory postsynaptic current (EPSC) is induced by two successive light pulses, which can emulate the excitatory postsynaptic current. The second peak EPSC (A_2) is significantly higher than the first peak EPSC (A_1), corresponding to the typical PPF phenomenon.[25] PPF behavior is quantified by a ratio called the PPF index (Q_{PPF}). As shown in Figure 2b, the PPF index depends on the light pulse interval time (t_{off}), which can be well fitted by the following formula:[26]

$$Q_{PPF} = \frac{A_2}{A_1} \tag{1}$$

$$Q_{PPF} = C_1 \exp\left(-\frac{t_{off}}{\tau_1}\right) + C_2 \exp\left(-\frac{t_{off}}{\tau_2}\right) + 1 \tag{2}$$

τ_1 and τ_2 represent the fast and slow decay behaviors, respectively. C_1 and C_2 are the facilitation magnitudes for the fast and slow decay behaviors, respectively. From Figure 2b, it is observed that the smaller pulse interval results in greater facilitation. As the t_{off} increased from 0.1 to 1.9 s, the PPF index value decreased from 158% to 110%. By Equation 2, τ_1 and τ_2 are derived to be 0.05 and 1.91 s, corresponding to the fast and slow decay time results, respectively, it can be seen that τ_1 is two orders of magnitude smaller than τ_2.[27] According to C_1 (0.29) and C_2 (0.55), the fast attenuation is easier to be achieved than the slow attenuation. The difference between slow and fast PPF attenuation can be thought of as an enhancement of biological

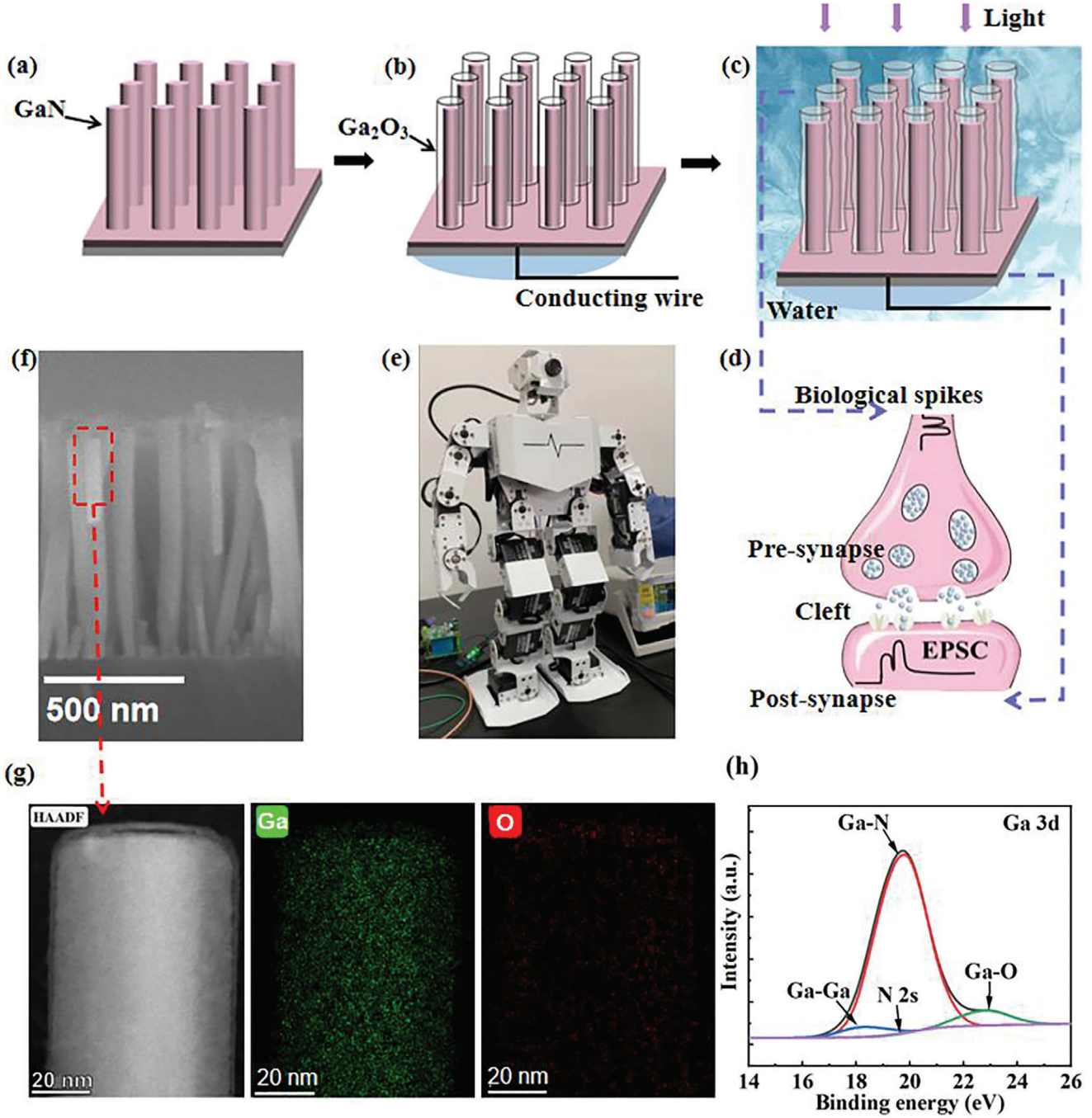

Figure 1. a) The growth of GaN nanowires. b) Ga_2O_3/GaN nanowires formed after oxidation and connected the conducting wire to the Si substrate. c) Measure the synaptic device under illumination. d) Schematic illustration of a biological synapse. e) The robot that works with the self-driven memristor synapse. f) SEM image of Ga_2O_3/GaN nanowires. g) A side-view image of enlarged Ga_2O_3/GaN hybrid nanowires and two images of AC-STEM high-resolution EDX mapping. (h) XPS spectrum of Ga_2O_3/GaN nanowires.

synaptic connections.[28] Moreover, the maximum PPF index value is larger than some other synaptic devices (**Table 1**),[23,29–31] indicating excellent performance. In the biological nervous system, a brief and slight increase in synaptic weight leads to the formation of short-term memory (STM). If repeating the stimulation, the weight of the biological synapses will continue to increase. After that, the STM will migrate from the hippocampus to the cerebral cortex and become long-term memory (LTM). From Figure 2c, the decay time of the synaptic device continues to rise with the increase of the light pulse number, corresponding to the continuous inflow of Ca^{2+} and the increase of the electrical conductivity in biological synapses. It indicates a transition from STM to LTM. Therefore, the self-driven Ga_2O_3/GaN synaptic devices have the ability to emulate the biological synapses.

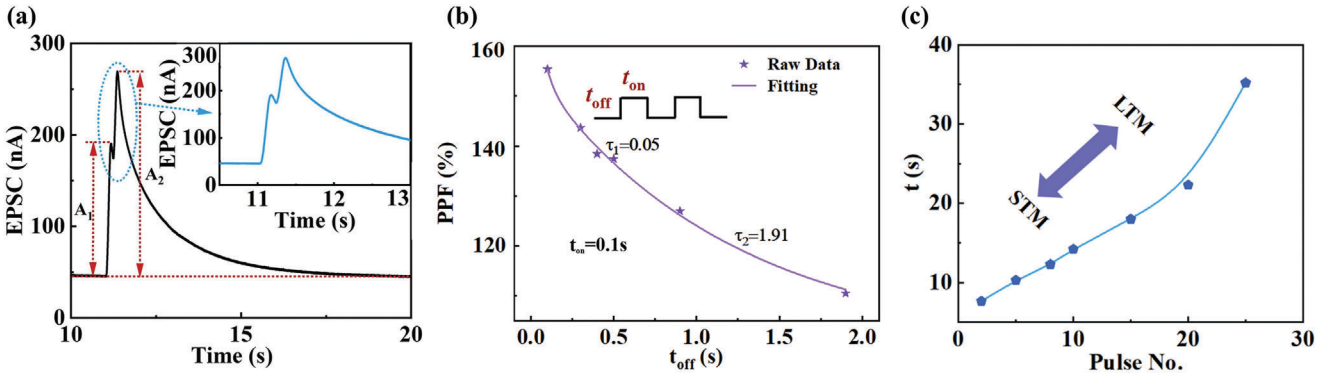

Figure 2. a) EPSC of the synaptic device triggered by two consecutive light pulses with a power density of 10.7 μW cm^{-2}. $t_{on} = t_{off} = 0.07$ s. b) PPF index at different t_{off}. t_{on} is 0.1 s and the bias voltage is 0 V. c) The decay time as a function of the number of light pulses. $t_{on} = t_{off} = 0.07$ s.

Inspired by biological synapses, the spike-timing-dependent plasticity (STDP) and spike-number-dependent plasticity (SNDP) of Ga_2O_3/GaN synaptic devices have been explored (**Figure 3a**). Small EPSC triggered by a short time (0.05 s) decays rapidly, while large EPSC triggered by a longer time (0.5 s) takes more time to reach the initial level, indicating a transition from STto LTM. In order to reach the same baseline level after six light pulses, the synaptic device exhibits a higher EPSC with a shorter t_{off} (Figure 3b). In Figure 3c, EPSC decreases progressively when the time interval (t_{off}) increases or the incident light power density decreases. When t_{on} and t_{off} are both 0.1 s, the EPSC results stimulated by 5 light pulses (Figure 3c) are higher than those stimulated by only 1 light pulse (Figure 3d), demonstrating the SNDP performance. In Figure 3d, EPSC increases when t_{on} increases because of the injection of more light photons. The light power density, t_{on}, and t_{off} are the key factors affecting EPSC results. Hence, the ability to transit from STM to LTM depends on the duration, frequency, pulse number, and light intensity of the light pulses, which reflects the synaptic plasticity of the device.

From the biological point of view, the increase and decrease of synaptic weight are the bases of the ability to learn and remember new information. Hence, synaptic weight is a metric to represent the memory level of the device, which is defined as the follows:

$$\Delta\omega = \frac{I_n - I_0}{I_0} \tag{3}$$

I_n represents the current after the stimulation of the number (n) light pulses. I_0 is the initial current. From **Figure 4a**, the synaptic weight increases with the increase of light-pulse number, which can emulate the learning process. In the first learning process, the synaptic weight increases from 65% to 97.5% after 7 pulses of light stimulation. In the second learning process, only 5 light pulses are required to make the synaptic weight return to the previous maximum. Such learning-forgetting-relearning behavior indicates the cognition or memory function.[32]

As shown in Figure 4b, with the increase of the light pulse number from 3 to 9, the photocurrent value can continuously increase and then become stable, which indicates that there is a saturation EPSC for a certain light power intensity. Similar characteristic can be achieved when increasing the light power density (Figure 4c). The higher light power density can make EPSC reach the saturation level easier. Obviously, the greater the light power density, the stronger the photocurrent intensity. In addition, when t_{off} and t_{on} increase from 0.1 to 1.0 s (Figure 4d), respectively, the corresponding photocurrent increases successively. As a result, the pulse number, light power density, t_{off}, and t_{on} are all the key parameters affecting the performance of synaptic devices significantly.

To better explain the underlying mechanism of the memristor synapse, the Ga_2O_3/GaN heterostructure and energy band diagrams are plotted in **Figure 5**. In the device, two conducting wires are connected to the EC workstation for measuring current (Figure 5a). The bandgap of Ga_2O_3 is 4.86 eV, corresponding to the light photon with a wavelength ≈255 nm.[33] A defined built-in potential difference and a stable built-in electric field are formed, which make the energy band of the semiconductor bend upward and finally form a Schottky barrier.[34] When the Ga_2O_3 section is in contact with the electrolyte, an electrochemical (EC) equilibrium is established by conveying electrons

Table 1. PPF index comparison among the memristor synapses based on III–V materials.

Materials	Maximum PPF index	Applied bias (V)	Self driven	Refs.
InGaAs nanowire with 140 nm P(VDF TrFE) film	225	0.4	No	[29]
InGaAs nanowire with 112 nm P(VDF TrFE) film	117	0.4	No	[29]
GaN/α-In_2Se_3 film	115	8	No	[30]
GaN microwires	108	3	No	[31]
GaN nanowires	130	3	No	[23]
Ga_2O_3 nanowires	158	0	Yes	This work

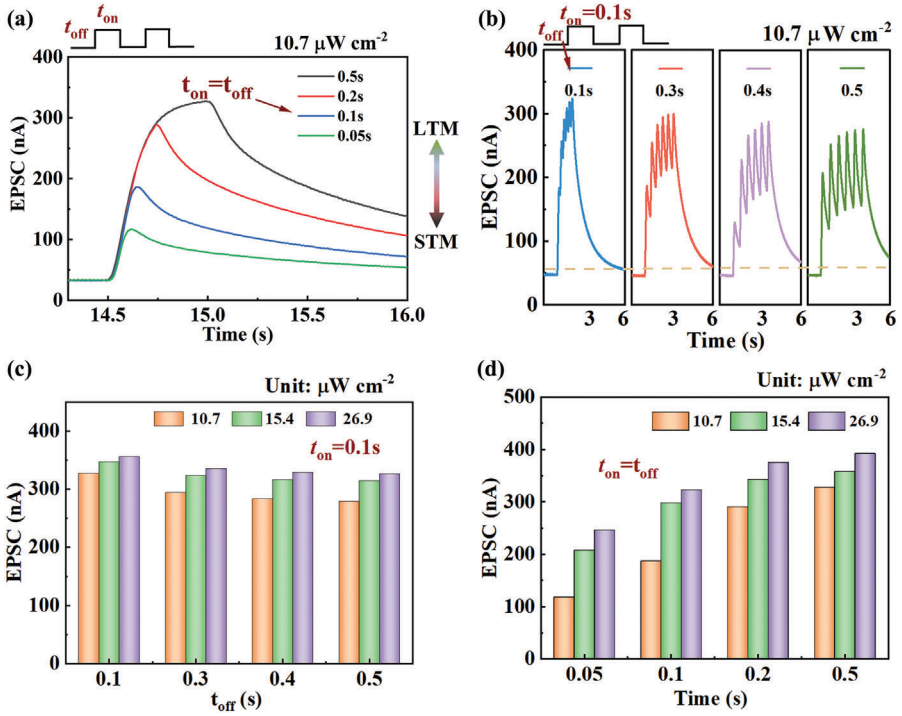

Figure 3. a) Dependence of the EPSC triggered by a light pulse (10.7 μW cm^{-2}) with different light-pulse widths. b) Dependence of the EPSC triggered by 6 light pulses (10.7 μW cm^{-2}) with different t_{off}. t_{on} is 0.1 s. c) EPSC triggered by 5 light pulses with different t_{off} and light power densities (from 10.7 to 26.9 μW cm^{-2}). t_{on} is 0.1 s. d) EPSC triggered by a light pulse with different t_{on} and light power densities (from 10.7 to 26.9 μW cm^{-2}). The t_{on} and t_{off} are the same.

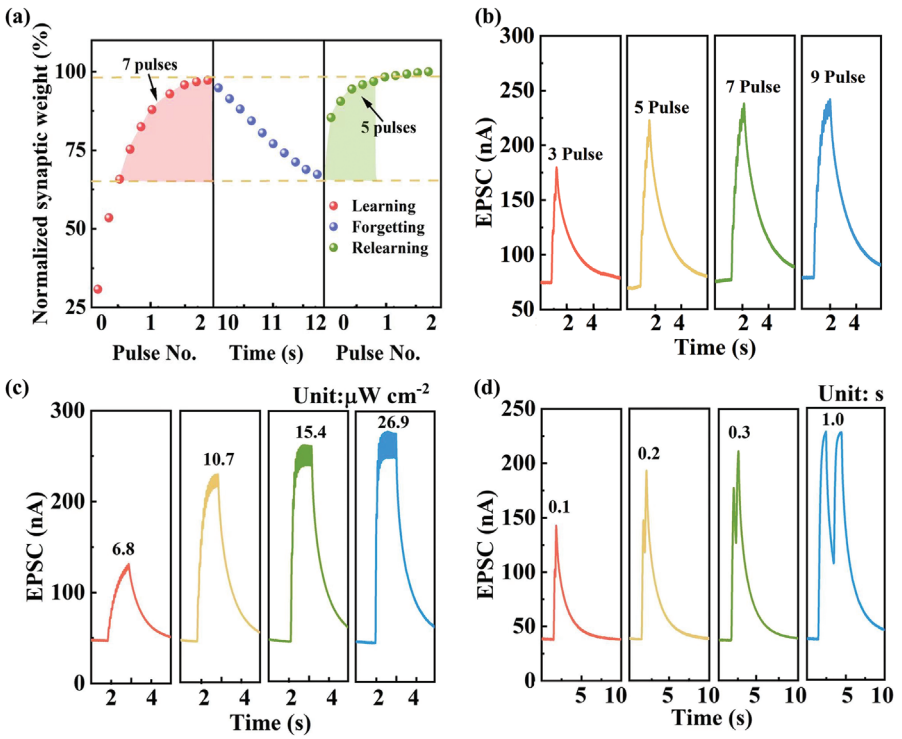

Figure 4. a) The learning-forgetting-relearning behavior of the synaptic device stimulated by continuous light pulses. The light power density is 10.7 μW cm^{-2}. t_{on} = t_{off} = 0.07 s. b) EPSC curves with different light-pulse numbers. The light power density is 10.7 μW cm^{-2}. t_{on} = t_{off} = 0.07 s. c) EPSC curves with different light power densities, where t_{on} = t_{off} = 0.07 s. d) EPSC curves with different t_{off} and t_{on}, where t_{on} = t_{off}. The operating bias of the device is 0 V.

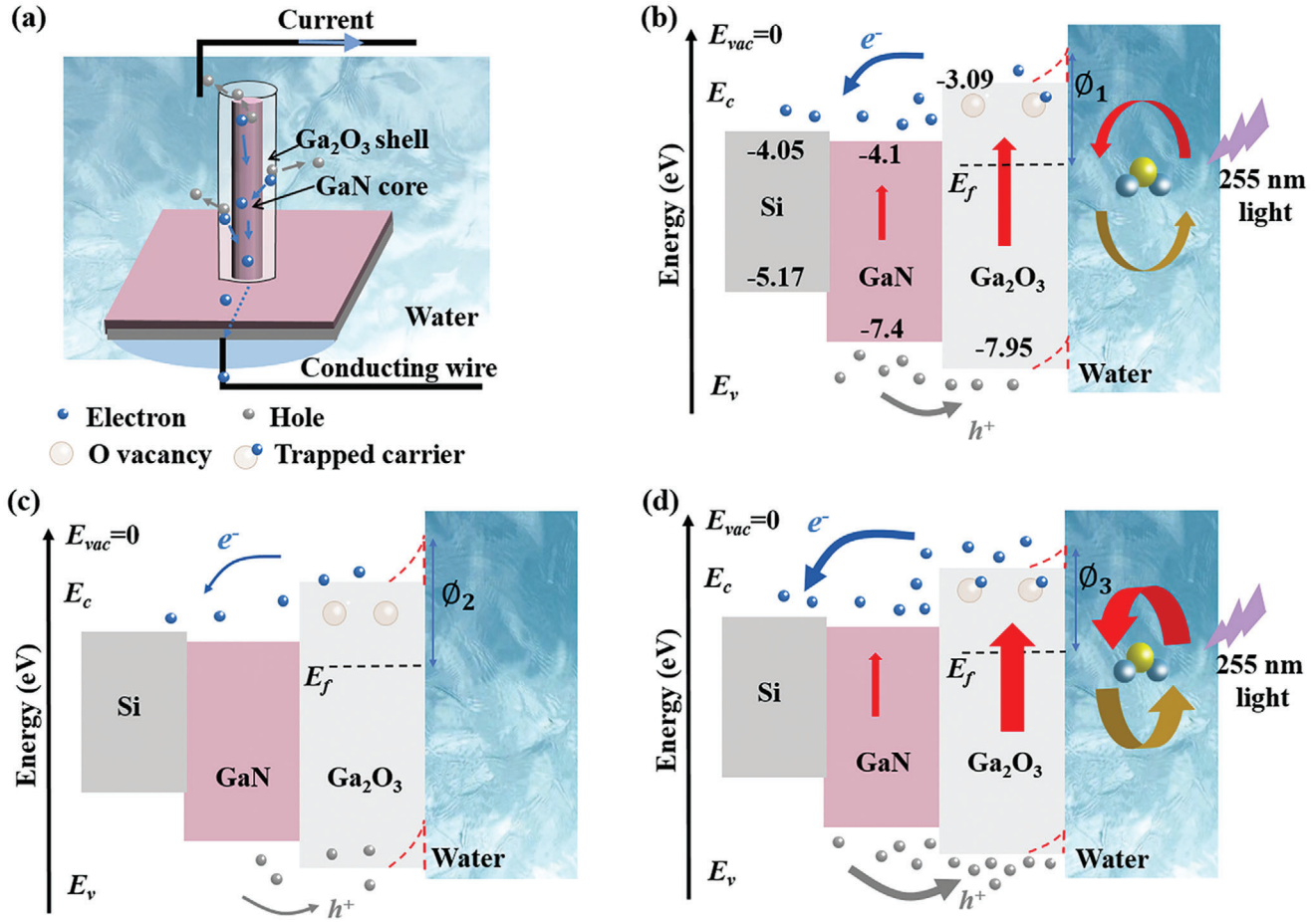

Figure 5. a) Schematic illustration of artificial synaptic device under UV illumination. Schematic energy band diagrams of the Ga_2O_3/GaN nanowires b) under the first 255 nm stimulation, c) without light stimulation, d) under the second 255 nm stimulation.

from the nanowires to the electrolyte, resulting in an upward band bend at the Ga_2O_3/GaN nanowire/electrolyte interface. Under dark conditions, band bending at the interface acts as an energy barrier to prevent carrier transport, resulting in a low dark current. When exposed to 255 nm light, the photocarriers generated in the Ga_2O_3 segment are prone to form a photocurrent by transporting them through the GaN/Ga_2O_3 core–shell nanowire heterojunctions (Figure 5a,b). The photogenerated holes move to the top nanowire region and the electrons move to the bottom nanowire region. The generation photocurrent may promote the splitting of water into hydrogen and oxygen through the following reactions:

$$4H^+ + 4\,e^- = 2H_2 \quad (4)$$

$$4h^+ + 2H_2O = O_2 + 4H^+ \quad (5)$$

Light harvesting and carrier transport can be accomplished without external bias in the entire circuit. As shown in Figure 5c, there may be some O-vacancy defects on the surface of heterogeneous structures. Specifically, oxygen ions may leave their original locations and enter gaps or pores in the nanowires, forming oxygen vacancies. At the same time, the carrier transfer reaction between metal ions and oxidants may also lead to the loss or excess of oxygen atoms, further forming O-vacancy defects.[35] These photogenerated charge carriers move through the material and may trigger or exacerbate the dislocations of oxygen ions, which can trap photogenerated carriers. After the removal of the light stimulus, the trapped carriers do not recombine immediately, making the EPSC of the device return to the initial state slowly (Figures 2a and 3b). Since there are still some carriers exist, the potential barrier will increase slightly ($Ø_2 > Ø_1$). When the same light stimulus is applied again (Figure 5d), more carriers and holes can be generated, resulting in a larger photocurrent (Figures 2a and 3b) and a lower potential barrier ($Ø_2 > Ø_1 > Ø_3$).

The schematic diagram of the whole system and the related circuit diagram are shown in **Figure** 6a. To operate the submerged synaptic device, we employ memristor synapses as a photoelectric conversion subsystem to capture light signals. This stimulation triggers electron transfer, resulting in a synaptic current that flows into the circuit via a metal plate. Within the circuit, the synaptic device corresponds to the yellow R_{NW} section with a memory effect. As illustrated in Figure 6b, a current–voltage (I–V) amplifier serves as the data acquisition subsystem to collect and amplify the weak analog current signals, corresponding to the green portion in the circuit diagram. The

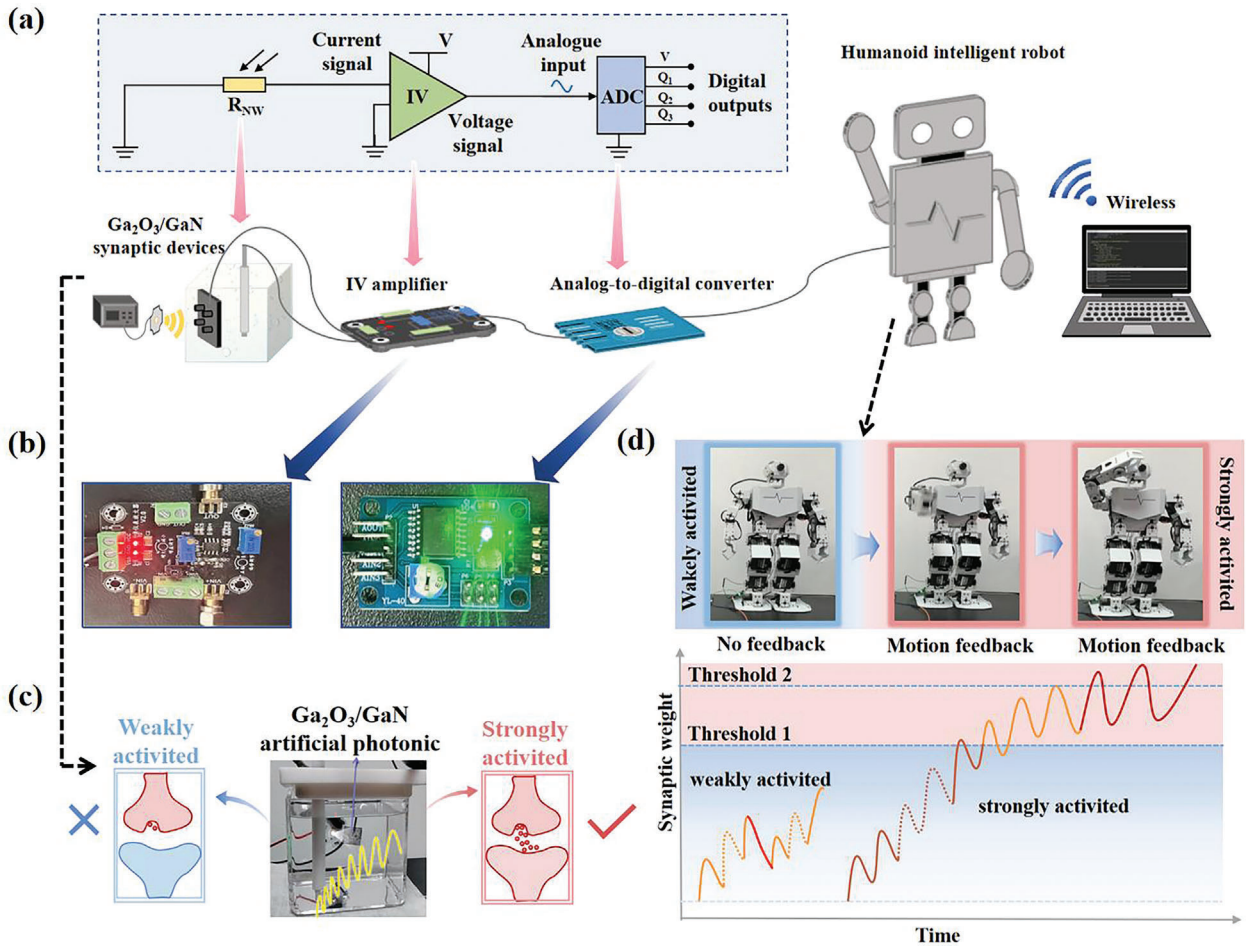

Figure 6. a) Schematic diagram of the control system of a humanoid intelligent robot. b) Physical images of IV amplifier and analog-to-digital converter. c) Schematic of threshold-dependent motion feedback driven by light stimuli. d) The artificial self-driven memristor synapse generates different electrical signals to drive the humanoid robot to make different actions under different light stimuli. The synaptic weight is schematic, but the robot images are real. In the experiments, the light frequency is 7 Hz and the bias voltage is 0 V. $t_{on} = t_{off} = 0.07$ s.

digital process is then executed by an analog-to-digital converter (ADC), which corresponds to the blue section in the circuit diagram. Concurrently, the application automatically sets and invokes the corresponding feedback, threshold parameters, and robotic actions. Ultimately, the signals originating from the synaptic devices are transmitted to the motion execution subsystem, which is programmed in Python to control the humanoid robot.

As shown in Figure 6c, when four light pulses are given (weak stimulus in the first stage), the EPSC signal does not reach the threshold. Thus, it is not possible to stimulate the postsynaptic membrane to generate action potentials, nor to further drive the humanoid robot to move (Figure 6d).[36] In other words, when the synaptic weight does not reach the first threshold, the robot does not respond at all. However, the EPSC signals can continue to accumulate and reach the firing threshold under 20-light-pulse stimulation (the second stage), leading to drive the humanoid robot to raise its hand (Video S1 and Figure 6d). Moreover, when the EPSC signal is enhanced to reach the second threshold by continuous light stimulation, the humanoid robot can be driven to make more intense movements, from raising a hand to waving a hand (the third stage). After the completion of the operation of waving hands, the humanoid robot lowers its hand and ends the operation. Notably, we can modulate the current thresholds and robot actions by Python programming. When receiving different light-pulse inputs, the artificial memristor synapse can result in the different motion feedback of the humanoid robot, performing the learning-experience behavior. In response to the control commands from the synaptic device, the humanoid robot can execute different actions. In addition, it is a way to improve the portability and expand the application scope of the device by replacing the water with the hydrogel,[19] which could be further studied. Therefore, the artificial synapse-based autonomous feedback system of humanoid robots performs a good collaboration of robot actions and bioinspired light sensation.

4. Conclusion

Here, we have proposed and demonstrated a self-driven memristor synapse utilizing Ga_2O_3 nanowires successfully, and further showcased its application in the manipulation of a humanoid

intelligent robot. In addition to exhibiting peak time-dependent plasticity, pulse facilitation, and memory learning capabilities, it is found that the self-driven memristor synapse based on Ga_2O_3 nanowires can achieve an excellent "learning-forgetting-relearning" functionality. By modulating the light stimulus conditions, the transition of the synaptic device can be facilitated from STM to LTM. In the artificial light-stimulated memristor synapse, the incident light, nanowire, and photogenerated carriers play the roles of the action potential, presynaptic membrane, and neurotransmitter in the biological synapse, respectively. The bending of the energy band and the presence of O-vacancies on the surface of Ga_2O_3 nanowires could be the principal factors contributing to the exceptional properties of artificial synaptic devices. On the other hand, the humanoid robot is capable of performing various actions in response to postsynaptic signals produced by the memristor synapse, such as raising and waving its robotic hand. Therefore, this research holds the promise of pioneering a novel domain within ultra-low-power AI systems, encompassing hardware-based neuromorphic computing and humanoid intelligent robots.

Supporting Information

Supporting Information is available from the Wiley Online Library or from the author.

Acknowledgements

J.Z., J.L., R.X., and Y.W. contributed equally to this work. This research was financially supported by the Key Research Program of Frontier Sciences, CAS (No. ZDBS-LY-JSC034), National Natural Science Foundation of China (No. 62174172), China Postdoctoral Science Foundation (Nos. 2023TQ0238 and 2023M742560) and Jiangsu Key Disciplines of the Fourteenth Five-Year Plan (No. 2021135). The authors are grateful for the technical support for Nano-X, Platform for Characterization & Test from Suzhou Institute of Nano-Tech and Nano-Bionics, Chinese Academy of Sciences (SINANO).

Conflict of Interest

The authors declare no conflict of interest.

Author Contributions

J.Z, J.L, R.X, and Y.W contributed equally to this work. J.Y.Z. completed all experiments in device fabrication. J.M.L. completed all device measurements and the corresponding data collections and analyses. Y.K.Z. conceived the idea. Y.K.Z. and J.Y.Z. guided the work. Y.K.Z., J.Y.Z. J.M.L. and R.X. completed the mechanism study. J.M.L., J.Y.Z., R.X. and Y.K.Z. wrote the original draft of this work. Y.K.Z. and J.Y.Z. carried out the funding acquisition and project administration. Y.K.Z. carried out all MBE experiments. R.X., J.W.W., and T.X.W. set the robot system. Y.D.W. and J.M.L. completed the video production. R.X., Y.D.W., J.M.L., J.W.W., and T.X.W. carried out the methodology and visualization of this work. R.X., Y.D.W., J.W.W., and T.X.W. performed the investigation. All authors reviewed this manuscript.

Data Availability Statement

The data that support the findings of this study are available from the corresponding author upon reasonable request.

Keywords

humanoid intelligent robot, light-stimulated synapse, Self-driven memristor synapse, ultralow power consumption, vertical Ga_2O_3 nanowires

Received: July 1, 2024
Revised: September 18, 2024
Published online:

[1] L. Qu, J. Ji, X. Liu, Z. Shao, M. Cui, Y. Zhang, Z. Fu, Y. Huang, G. Yang, W. Feng, *Nanotechnology* **2023**, *34*, 225203.
[2] X. Pi, D. Yang, Y. Li, Y. Wang, *Sci Sin Inform* **2020**, *50*, 892.
[3] Y. Jiang, X. Ma, L. Wang, J. Zhang, Z. Wang, R. Zhao, G. Liu, Y. Li, C. Zhang, C. Ma, Y. Qi, L. Wu, J. Gao, *Phys. Rev. Lett.* **2023**, *130*, 196801.
[4] Y. Wang, L. Yin, W. Huang, Y. Li, S. Huang, Y. Zhu, D. Yang, X. Pi, *Adv. Intell. Syst.* **2020**, *3*, 2000099.
[5] Z. Feng, J. Yu, Y. Wei, Y. Wang, B. Tian, Y. Li, L. Cheng, Z. Wang, Q. Sun, *Brain-X* **2023**, *1*, e24.
[6] J. Guo, W. Li, J. Zheng, Y. Liao, Y. Shen, J. Zhao, K. Wang, C. Wu, T. Guo, *J. Vac. Sci. Technol.* **2021**, *8*, 699.
[7] S. Ling, C. Zhang, C. Ma, Y. Li, Q. Zhang, *Adv. Funct. Mater.* **2022**, *33*, 2208320.
[8] J. Y. Kwon, J. E. Kim, J. S. Kim, S. Y. Chun, K. Soh, J. H. Yoon, *Exploration* **2023**, *4*, 20220162.
[9] N. Ilyas, J. Wang, C. Li, D. Li, H. Fu, D. Gu, X. Jiang, F. Liu, Y. Jiang, W. Li, *Adv. Funct. Mater.* **2021**, *32*, 2110976.
[10] F. Huang, F. Fang, Y. Zheng, Q. You, H. Li, S. Fang, X. Cong, K. Jiang, Y. Wang, C. Han, W. Chen, Y. Shi, *Nano Res.* **2022**, *16*, 1304.
[11] Y. Deng, S. Liu, M. Li, N. Zhang, Y. Feng, J. Han, Y. Kapitonov, Y. Li, T. Zhai, *Chip* **2024**, *3*, 100088.
[12] Y. Tong, H. Liu, Z. Zhang, *IEEE/CAA J. Automatica Sinica* **2024**, *11*, 301.
[13] J. Li, Z. Shen, Y. Cao, X. Tu, C. Zhao, Y. Liu, Z. Wen, *Nano Energy* **2022**, *103*, 107744.
[14] M. Lee, W. Park, H. Son, J. Seo, O. Kwon, S. Oh, M. G. Hahm, U. J. Kim, B. Cho, *APL Mater.* **2021**, *9*, 031103.
[15] X. Lin, H. Long, S. Ke, Y. Wang, Y. Zhu, C. Chen, C. Wan, Q. Wan, *Chin. Phys. Lett.* **2022**, *39*, 068501.
[16] K. Sato, Y. Hayashi, N. Masaoka, T. Tohei, A. Sakai, *Sci. Rep.* **2023**, *13*, 1261.
[17] T. He, X. Zhang, X. Ding, C. Sun, Y. Zhao, Q. Yu, J. Ning, R. Wang, G. Yu, S. Lu, K. Zhang, X. Zhang, B. Zhang, *Adv. Opt. Mater.* **2019**, *7*, 1801563.
[18] M. Jiang, J. Zhang, W. Yang, D. Wu, Y. Zhao, Y. Wu, M. Zhou, S. Lu, *Adv. Mater. Interfaces* **2022**, *9*, 2200028.
[19] J. Zhang, B. Jiao, J. Dai, D. Wu, Z. Wu, L. Bian, Y. Zhao, W. Yang, M. Jiang, S. Lu, *Nano Energy* **2022**, *100*, 107437.
[20] S. L. Jackman, W. G. Regehr, *Neuron* **2017**, *94*, 447.
[21] R. S. Zucker, W. G. Regehr, *Annu. Rev. Physiol.* **2002**, *64*, 355.
[22] Y. Li, Q. Qian, X. Zhu, Y. Li, M. Zhang, J. Li, C. Ma, H. Li, J. Lu, Q. Zhang, *InfoMat* **2020**, *2*, 995.
[23] C.-H. Huang, C.-Y. Wu, Y.-F. Lin, Y.-C. Chou, K.-T. Lee, *Adv. Funct. Mater.* **2023**, *33*, 2306030.
[24] X. Chen, B. Chen, B. Jiang, T. Gao, G. Shang, S. T. Han, C. C. Kuo, V. A. L. Roy, Y. Zhou, *Adv. Funct. Mater.* **2022**, *33*, 2208807.
[25] H. Chen, H. Huang, *Acta Polym. Sin.* **2022**, *53*, 374.
[26] C. Mahata, J. Park, M. Ismail, S. Kim, *J. Alloys Compd.* **2023**, *938*, 168539.
[27] S. Karthikeyan, S. W. Johnston, D. Gayakwad, S. Mahapatra, R. J. Bodnar, J. Zhao, R. Joshi, M. K. Hudait, *Nanoscale* **2024**, *15*, 7225.
[28] S. M. Kwon, S. W. Cho, M. Kim, J. S. Heo, Y. H. Kim, S. K. Park, *Adv. Mater.* **2019**, *31*, 1906433.

[29] P. Xie, Y. Huang, W. Wang, Y. Meng, Z. Lai, F. Wang, S. Yip, X. Bu, W. Wang, D. Li, J. Sun, J. C. Ho, *Nano Energy* **2021**, *91*, 106654.
[30] J. Y. Yang, M. Park, M. J. Yeom, Y. Baek, S. C. Yoon, Y. J. Jeong, S. Y. Oh, K. Lee, G. Yoo, *ACS Nano* **2023**, *17*, 7695.
[31] Q. Hua, X. Cui, H. Liu, C. Pan, W. Hu, Z. L. Wang, *Nano Lett.* **2020**, *20*, 3761.
[32] Y. Li, S. Ling, R. He, C. Zhang, Y. Dong, C. Ma, Y. Jiang, J. Gao, J. He, Q. Zhang, *Nano Res.* **2023**, *16*, 11278.
[33] S. Li, Y. Zhi, C. Lu, C. Wu, Z. Yan, Z. Liu, J. Yang, X. Chu, D. Guo, P. Li, Z. Wu, W. Tang, *J. Phys. Chem. Lett.* **2020**, *12*, 447.
[34] F. Schäffler, G. Abstreiter, *J. Vac. Sci. Technol., B: Microelectron. Process. Phenom.* **1985**, *3*, 1184.
[35] Z. Wang, R. Lin, Y. Huo, H. Li, L. Wang, *Adv. Funct. Mater.* **2022**, *32*, 2109503.
[36] T. Fu, X. Liu, S. Fu, T. Woodard, H. Gao, D. R. Lovley, J. Yao, *Nat. Commun.* **2021**, *12*, 3351.